V International Conference on Particle-based Methods – Fundamentals and Applications
PARTICLES 2017
P. Wriggers, M. Bischoff, E. Oñate, D.R.J. Owen, & T. Zohdi (Eds)

NUMERICAL SIMULATION OF THE SEDIMENTATION OF AN ELLIPTIC PARTICLE UNDER EXTERNAL ELECTRIC FIELD USING ISPH

NIMA TOFIGHI[1], MEHMET YILDIZ[2] AND AFZAL SULEMAN[1]

[1] Department of Mechanical Engineering, University of Victoria, Victoria, BC V8P 5C2, Canada
ntofighi@uvic.ca; suleman@uvic.ca

[2] Integrated Manufacturing Technologies Research and Application Center, Faculty of Engineering and Natural Sciences (FENS), Sabanci University, Tuzla, 34956 Istanbul, Turkey
meyildiz@sabanciuniv.edu

Key words: Smoothed Particle Hydrodynamics, Fluid-Structure Interaction, Electrohydrodynamics

Abstract. Incompressible smoothed particle hydrodynamics method has been used to simulate the sedimentation of a two-dimensional rigid elliptic disc in quiescent medium in presence of an external electric field. The motion of the elliptic disc in the absence of the electric field is compared to literature data and good agreement is observed. The results show that the trajectory of the elliptic disc in presence of the electric field is strongly affected by the electrical properties of fluid and solid.

1 Introduction

This study deals with the motion of a rigid elliptic particle sedimenting in a quiescent background fluid. At low Reynolds numbers, the particle tends to sediment lying flat on its major axis [1]. When placed in an external electric field, the electrical forces exerted on the particle may result in a moment that changes its orientation [2]. The electric field induced rotation in this case is of particular significance in particle orientation in sprays or microfluidic devices, to name a few [3, 4].

Electrohydrodynamics of multiphase flows have been successfully investigated using incompressible smoothed hydrodynamics (ISPH) method before [5]. Here, an isothermal two dimensional ISPH method is used to calculate velocity, pressure and electrical potential of the elliptic particle and its surrounding fluid. The sedimentation of an elliptic particle in the absence of the external electric field has been investigated before in [1, 6] and our method is validated in [7].

The sedimentation pattern of the elliptic particle is highly dependent on the electrical properties of the system and proximity of the boundaries. To investigate the long term

sedimentation patterns, a shifting boundary condition is implemented and tested without the electric field. Then, four sets of boundary conditions and two different sets of electrical properties are simulated and the behavior of the elliptic particle is investigated.

2 Governing Equations and Geometry

Equations governing an incompressible flow subject to an external electric field may be written in dimensionless form as

$$\boldsymbol{\nabla} \cdot \mathbf{u} = 0, \tag{1}$$

$$\rho \frac{\mathrm{D}\mathbf{u}}{\mathrm{D}t} = \boldsymbol{\nabla} p + \frac{1}{\mathrm{Re}} \boldsymbol{\nabla} \cdot \boldsymbol{\tau} + \frac{1}{\mathrm{Eg}} \mathbf{f}_{(e)}, \tag{2}$$

where $\mathbf{u}$ is the velocity vector, p is pressure, ρ is density, t is time and $\mathrm{D}/\mathrm{D}t = \partial/\partial t + \mathbf{u} \cdot \boldsymbol{\nabla}$ represents the material time derivative. Here, $\boldsymbol{\tau}$ is the viscous stress tensor,

$$\boldsymbol{\tau} = \mu \left[\boldsymbol{\nabla}\mathbf{u} + (\boldsymbol{\nabla}\mathbf{u})^{\dagger} \right], \tag{3}$$

where μ denotes viscosity and superscript $\square^{\dagger}$ represents the transpose operation. $\mathbf{f}_{(e)}$ is the electric force vector defined as [8]

$$\mathbf{f}_{(e)} = -\frac{1}{2} \mathbf{E} \cdot \mathbf{E} \boldsymbol{\nabla} \varepsilon + q^{v} \mathbf{E}. \tag{4}$$

Here ε denotes electric permittivity, q^{v} is is the volume charge density near the interface while $\mathbf{E}$ is the electric field vector. Assuming small dynamic currents and neglecting magnetic induction effects, the electric field is irrotational [8] and may be represented by gradient of an electric potential ϕ, $\mathbf{E} = -\boldsymbol{\nabla}\phi$. Further assumption of fast electric relaxation time compared to viscous relaxation time leads to the following relations for electric potential and charge density

$$\boldsymbol{\nabla} \cdot (\sigma \boldsymbol{\nabla} \phi) = 0, \tag{5}$$

$$q^{v} = \boldsymbol{\nabla} \cdot (\varepsilon \boldsymbol{\nabla} \phi), \tag{6}$$

where σ is the electrical conductivity.

Dimensionless values are formed using the following scales

$$\begin{aligned} &\mathbf{x} = \mathbf{x}^{*}/d, \quad \rho = \rho^{*}/\rho_{f}, \quad \mathbf{u} = \mathbf{u}^{*}/\sqrt{gd}, \\ &t = t^{*}\sqrt{g/d}, \quad \mathbf{E} = \mathbf{E}^{*}/E_{\infty}, \quad \phi = \phi^{*}/E_{\infty}H, \\ &p = (p - \rho \mathbf{g} \cdot \mathbf{x})^{*}/\rho_{f} g d, \quad \mathcal{D} = \rho_{s}/\rho_{f}, \quad \mathcal{V} = \mu_{s}/\mu_{f}, \\ &\mathcal{P} = \varepsilon_{s}/\varepsilon_{f}, \quad \mathcal{C} = \sigma_{s}/\sigma_{f}, \end{aligned} \tag{7}$$

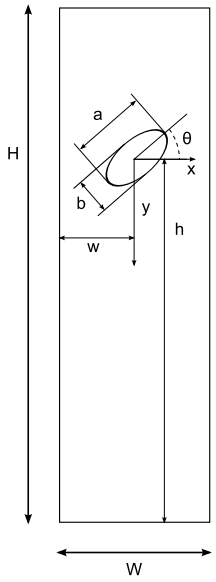

Figure 1: General schematic of the test cases

leading to Reynolds and Electrogravitational numbers defined as

$$\mathrm{Re} = \frac{\rho_f \sqrt{g d^3}}{\mu_f}, \quad \mathrm{Eg} = \frac{\rho_f g d}{\varepsilon_f E_\infty^2}. \tag{8}$$

Here E_∞ is the undisturbed electric field intensity, H is the distance between electrodes and $d = \sqrt{ab}$ denotes equivalent ellipse diameter. An asterisk marks dimensional variables whereas subscripts $\square_s$ and $\square_f$ denote fluid and solid phases, respectively.

Figure 1 shows the general geometry of the cases studied here. The elliptic particle is positioned at (w, h) in a $W \times H$ rectangular box at an angle θ with respect to the horizontal axis. Aspect ratio of the ellipse is set to $a/b = 2$. Gravitational acceleration acts in positive y direction. When electric field is present, an electric potential difference of $\Delta\phi = E_\infty H$ is imposed between horizontal walls, generating an undisturbed electric field parallel to side walls. Details of initial particle arrangement are given in [7].

3 Numerical Method

To distinguish between different phases, a color function $\hat{c}$ is defined such that it assumes a value of zero for one phase and unity for the other. The color function is then smoothed out across the phase boundaries as

$$c_{\mathrm{i}} = \sum_{\mathrm{j}=1}^{J_n} \frac{\hat{c}_{\mathrm{j}} W_{\mathrm{ij}}}{\psi_{\mathrm{i}}}, \tag{9}$$

to ensure smooth transition between the properties of each phase when used for their interpolation. Here, $\psi_{\mathrm{i}} = \sum_{\mathrm{j}=1}^{J_n} W_{\mathrm{ij}}$, is the number density of SPH particle i, calculated

as the sum of interpolation kernel of neighboring particles i and j over all neighbors of particle i, J_n. Interpolation kernel, $W(r_{\mathrm{ij}}, h)$, is a function of the magnitude of distance vector $\mathbf{r}_{\mathrm{ij}} = \mathbf{r}_{\mathrm{i}} - \mathbf{r}_{\mathrm{j}}$ and smoothing length h [9]. Interpolation of phase properties is carried out through

$$\frac{1}{\chi_{\mathrm{i}}} = \frac{c_{\mathrm{i}}}{\chi_s} + \frac{1 - c_{\mathrm{i}}}{\chi_f}, \tag{10}$$

where χ may denote density, viscosity, permittivity or conductivity.

The solid region is treated as a liquid with a viscosity ratio of $\mathcal{V} = 100$ [7]. Additionally, rigidity constraints are imposed by computing a center-of-mass velocity and angular velocity

$$\mathbf{u}_s = \frac{1}{J_s} \sum_{\mathrm{j}=1}^{J_s} \mathbf{u}_{\mathrm{j}}, \quad \omega_s = \frac{1}{I_s} \sum_{\mathrm{j}=1}^{J_s} \mathbf{u}_{\mathrm{j}} \times \mathbf{r}_{\mathrm{j}s}, \tag{11}$$

which are used to assign an individual velocity to each solid particle according to

$$\mathbf{u}_{\mathrm{i}} = \mathbf{u}_s + \omega_s \times \mathbf{r}_{\mathrm{i}s}. \tag{12}$$

Here, $\mathbf{r}_{\mathrm{i}s} = \mathbf{r}_{\mathrm{i}} - \mathbf{r}_s$ where $\mathbf{r}_s$ denotes the solid object's center of mass, J_s is the number of particles present in the solid phase and I_s is the solid object's moment of inertia about its center of mass.

A predictor-correcter scheme is employed to advance the governing equations in time with a variable timestep according to $\Delta t = 0.25h/u_{max}$, where u_{max} is the largest particle velocity magnitude [10]. In the predictor step, (5) and (6) are solved to obtain $\mathbf{f}_{(e)}^{(n)}$ through (4). Then positiona and velocity are advanced to their intermediate forms using the following relations,

$$\mathbf{r}_{\mathrm{i}}^{+} = \mathbf{r}_{\mathrm{i}}^{(n)} + \mathbf{u}_{\mathrm{i}}^{(n)} \Delta t + \boldsymbol{\delta}\mathbf{r}_{\mathrm{i}}^{(n)}, \tag{13}$$

$$\mathbf{u}_{\mathrm{i}}^{+} = \mathbf{u}_{\mathrm{i}}^{(n)} + \left(\frac{1}{\mathrm{Re}} \boldsymbol{\nabla} \cdot \boldsymbol{\tau}_{\mathrm{i}}^{(n)} + \frac{1}{\mathrm{Eg}} \mathbf{f}_{(e),\mathrm{i}}^{(n)} \right) \frac{\Delta t}{\rho_{\mathrm{i}}}, \tag{14}$$

where starred variables represent intermediate values and superscript (n) denotes values at the nth time step. Number density and fluid properties are calculated according to the intermediate position of the interface. The artificial particle displacement vector in (13), $\boldsymbol{\delta}\mathbf{r}_{\mathrm{i}}$, is defined as in [10] and a constant value of 0.06 is used.

Using intermediate values, pressure at the next time step is calculated and positions and velocities are advanced in time using the following equations

$$\boldsymbol{\nabla} \cdot \left(\frac{1}{\rho_{\mathrm{i}}^{+}} \boldsymbol{\nabla} p_{\mathrm{i}}^{(n+1)} \right) = \frac{\boldsymbol{\nabla} \cdot \mathbf{u}_{\mathrm{i}}^{+}}{\Delta t}, \tag{15}$$

$$\mathbf{u}_{\mathrm{i}}^{(n+1)} = \mathbf{u}_{\mathrm{i}}^{+} - \frac{1}{\rho_{\mathrm{i}}} \boldsymbol{\nabla} p_{\mathrm{i}}^{(n+1)} \Delta t, \tag{16}$$

Table 1: Configurations for testing the shifting boundary condition.

Case	A	B	C	D
Top and bottom	No-slip	Shifting	No-slip	Shifting
Side walls	No-slip	No-slip	Periodic	Periodic

$$\mathbf{r}_{\mathrm{i}}^{(n+1)} = \mathbf{r}_{\mathrm{i}}^{(n)} + \frac{1}{2}\left(\mathbf{u}_{\mathrm{i}}^{(n)} + \mathbf{u}_{\mathrm{i}}^{(n+1)}\right)\Delta t + \boldsymbol{\delta}\mathbf{r}_{\mathrm{i}}^{(n)}. \tag{17}$$

In these equations, the rigidity constraints ((11) and (12)) are implemented after each velocity update.

Details of the spatial discretization and enforcement of boundary conditions are given in [7].

4 Results

4.1 Shifting boundary condition

A sedimenting ellipse is likely to move in a periodic manner. However, the period of such motion may be very long and the effects of bounding walls may be substantial. As such, the long-term simulation of the sedimentation of the elliptic particle may be necessary for observing the periodic motion in some cases. To implement the shifting boundary, the ellipse is placed at the center of the computational domain. As its center of mass moves up by one particle spacing, all particles are shifted so that the ellipse is vertically centered. Any particles transfered out of the upper boundary are discarded and a new layer of particles are added at the bottom boundary. If the computational domain is high enough, the ellipse will continue its descent without limitation.

Since the motion of the ellipse without electric field is well studied, the method is tested in the absence of an external electric field [1, 6, 7]. The parameters are set as $\mathcal{D} = 1.1$, $\mathrm{Re} = 58.8$, $a/b = 2$, $W/a = 4$, $h/d = 34$ and $\theta = \pi/4$. Computational domain is discretized by 80035 particles. The combination of the boundary conditions used here are given in table 1.

In most cases, the effects of top and bottom walls should not contaminate the results and the simulations are terminated before wall effects appear. However, the effects of side walls are unavoidable in sedimentation in confined domains [1]. In this sense configurations A-B and C-D are paired for comparison. It is expected that cases B and D behave similar to cases C and D as long as the ellipse is far from the bottom wall. Figure 2 plots the horizontal position and orientation of the particle with respect to its vertical position. Cases A and C reach the bottom wall at $y^*/W = 6$ while cases B and D may continue indefinitely. The agreement between A-B and C-D pairs is excellent and this means that from a hydrodynamic point of view, the implementation of the shifting boundary has no effect on the sedimentation. It is worth mentioning that in all cases, the ellipse comes to a horizontal orientation while its position is dependent on the side wall boundary condition. With a no-slip wall, the hydrodynamic forces move the ellipse toward the center of the

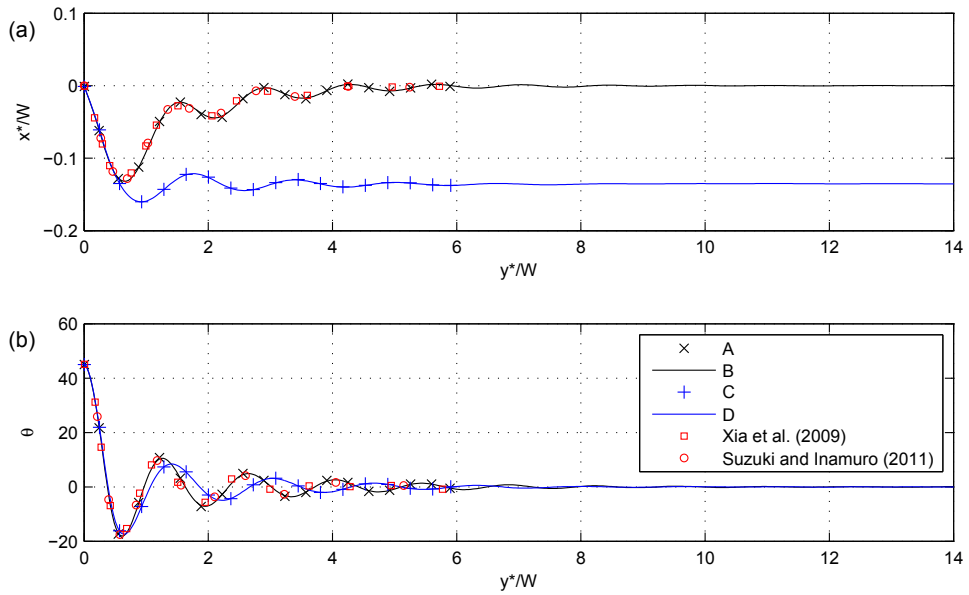

Figure 2: Horizontal position (a) and orientation (b) of the elliptic disc while sedimenting.

domain while in the periodic configuration, the ellipse settles further away from its starting horizontal position. The Reynolds numbers based on terminal velocity, $\mathrm{Re}_t = \rho_f u_t d/\mu_f$, is equal to 15.1 and 16.2 for A-B and C-D pairs, respectively. As expected, this shows that the ellipse descends slower in confined domain due to wall effects.

4.2 Boundary effects on sedimentation

The introduction of the electrical field may significantly alter the behavior of the ellipse sedimenting in quiescent fluid. Two sets of permittivity ratio and conductivity ratio pairs of $(10, 20)$ and $(20, 0.1)$ are used and will be referred to as cases S and U, respectively. The significance of the electrical parameters chosen is that the former has $\tau_s < \tau_f$ while the latter has $\tau_s > \tau_f$, where $\tau = \varepsilon/\sigma$. This means that the electrical forces resist rotation for case S while the situation for case U is more complex. Velocity boundary conditions are as given in table 2. For configurations A and B no electric field lines pass through the side walls while in configurations C and D, the side walls are periodic. Reynolds number is set to 58.8 while Electrogravitational number is equal to 27.7.

Figure 3 plots the horizontal position and orientation of the ellipse versus its vertical position for S cases. In all cases, the ellipse aligns itself with the electric field almost instantly, regardless of the boundary configuration, with cases A-B and C-D following the same trajectory. When side walls are present, *i.e.* configurations A and B, the ellipse moves slowly toward the center of the computational domain whereas in configurations C and D, the ellipse remains to the right of its starting horizontal position. It is worth noting that the early horizontal deviation in electrified cases is in the opposite direction

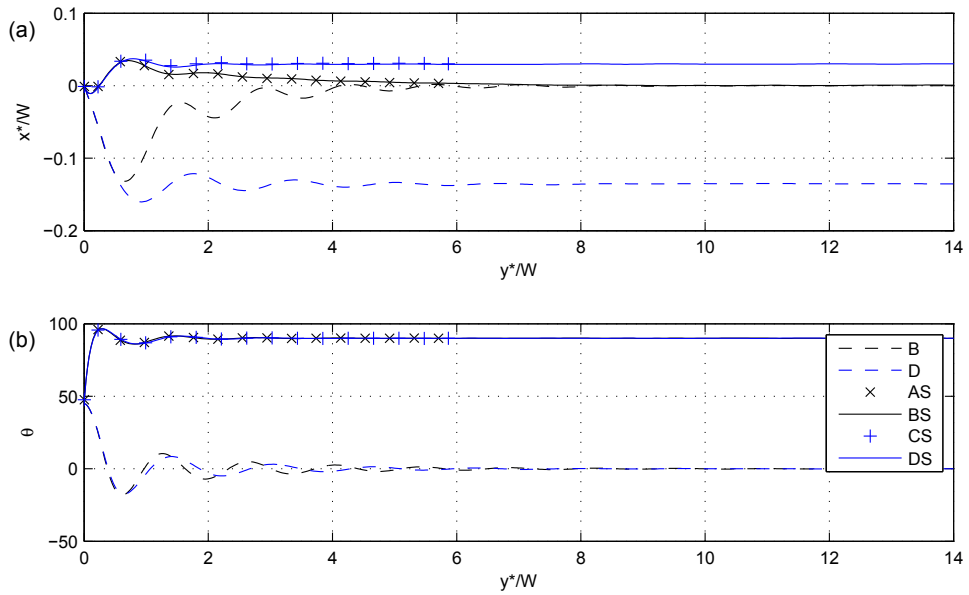

Figure 3: Horizontal position (a) and orientation (b) of the elliptic disc of case S while sedimenting in an external electric field.

of the cases without the electric field.

Figure 4 provides the horizontal position and orientation of the ellipse for case U. Unlike case S, case U shows remarkably different trajectories with different boundary configurations. While cases CU and DU behave similarly with a periodic motion, cases AU and BU are completely unrelated. This shows that the electrical boundaries have notable effects when there is a race between $\mathbf{f}_{(ep)} = -\mathbf{E}\cdot\mathbf{E}\boldsymbol{\nabla}\varepsilon/2$ and $\mathbf{f}_{(eq)} = q^v\mathbf{E}$ (equation (4)). Cases CU and DU follow a periodic trajectory to the left of their starting position and rotate up to ten degrees around the flat orientation. Case BU follows a periodic motion of equal horizontal distance and angular span to that of CU and DU at a higher frequency in the center of the channel. Unlike others, case AU does not follow a periodic trajectory and stays mostly in an upright orientation. It moves back and forth near the left wall before changing direction in $y^*/W = 4$ and heading toward the right wall.

Table 2 provides Re_t for all cases. For oscillating cases, the average vertical velocity is used instead of the terminal velocity in computation of Re_t. In agreement with the observations made above, cases AS-BS and CS-DS have similar terminal Reynolds numbers. For case U, the oscillatory motion reduces the descent velocity resulting in smaller Re_t. As expected, cases CU and DU have similar terminal Reynolds numbers while the largest Re_t belongs to AU which descends in a mostly upright orientation.

To explore the effects of the electrical forces on the motion of case U in more detail, figures 5 and 6 provide the torques and horizontal component of the forces applied to the ellipse during its descent. The electrical force and torque are computed directly from the electrical forces applied to particles of the solid phase. Since the FSI coupling technique

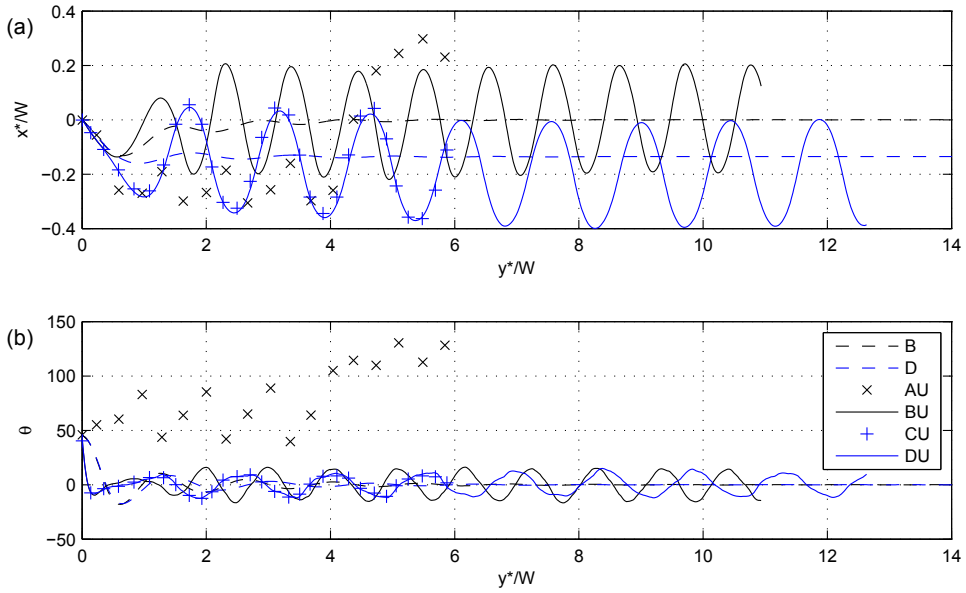

Figure 4: Horizontal position (a) and orientation (b) of the elliptic disc of case U while sedimenting in an external electric field.

Table 2: Terminal Reynolds number Re_t for cases S and U for different boundary configurations. When no electric field is applied $\mathrm{Re}_t = 15.1$ [7].

Case	A	B	C	D
S	22.1	21.9	22.8	22.8
U	19.7	9.6	11.1	11.2

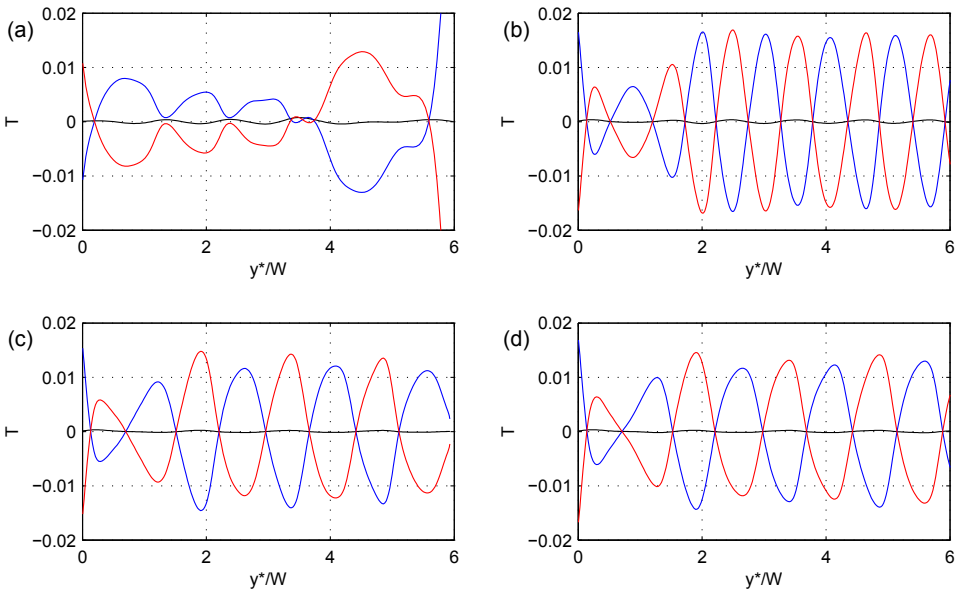

Figure 5: Hydrodynamic torque (blue), electric torque (red) and resultant torque applied to the ellipse of case U with boundary configurations of A (a), B (b), C (c) and D (d) while sedimenting in an external electric field. A positive value induces a counter-clockwise rotation.

used here does not provide an explicit interface for the solid body, the hydrodynamical parts are found by subtracting the electrical components from the resultant torque and force applied to the body. The resultant components are calculated using the position and orientation of the ellipse in time. The results are smoothed using a Gaussian filter to remove spurious oscillations.

The differences between case AU and other cases are apparent in both torque and forces exerted on it. Having both side and top boundaries in its vicinity, the initial electrical torque turns the ellipse in counter-clockwise direction to align it with the electric field. The hydrodynamic torque is comparable but smaller than the electrical counterpart and the ellipse maintains its orientation. This causes it to approach the left wall where it is deflected due to electrical forces ($y^*/W \approx 0.75$). While descending near the wall from $y^*/W \approx 1$ to 4, the electric torque encourages a flat orientation whereas the hydrodynamic torque opposes it. The ellipse gets closer to the left wall progressively with each approach and this reduces the hydrodynamic forces pushing it toward the wall. At $y^*/W \approx 4$, the ellipse breaks off the left wall and heads toward the opposing wall. While passing the middle of the channel, the electrical and hydrodynamical forces become negligible. At this position, electrical torque encourages a counter-clockwise rotation while a slightly larger hydrodynamical torque resists it. After $y^*/W \approx 5$, the bottom wall affects the simulation.

Despite sharing the same side wall configuration with case AU, replacing top and bottom boundaries with shifting walls changes the electrical effects exerted on case BU

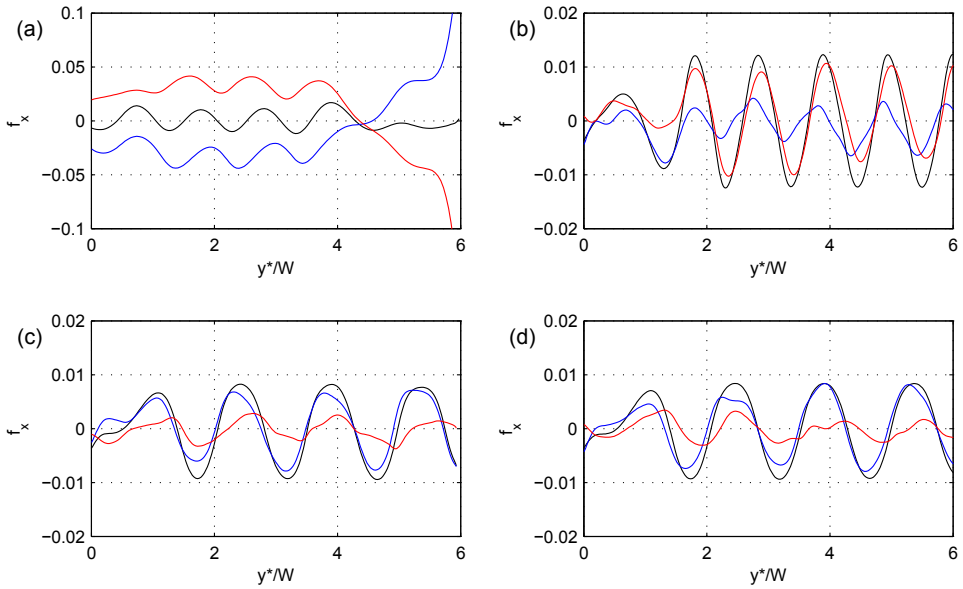

Figure 6: Horizontal component of hydrodynamic force (blue), electric force (red) and resultant force applied to the ellipse of case U with boundary configurations of A (a), B (b), C (c) and D (d) while sedimenting in an external electric field. A positive value moves the ellipse to the right.

significantly. Throughout its path, the electrical torque remains the dominant term and dictates both rotation and horizontal position. Initially, the electrical torque turns the ellipse toward a flat orientation while the hydrodynamic torque resists it. The electrical torque is clockwise for positive angles and counter-clockwise for negative angles. Electrical and hydrodynamic forces are in agreement and act to move the ellipse away from the wall. The period of both forces are similar while the electric component lags behind the hydrodynamic part.

Cases CU and DU act in a similar fashion. The electrical and hydrodynamical torques alternate as the ellipse pivots around its flat orientation. The torques oppose each other with the electrical torque as the dominant component. On the other hand, the dominant force term is the hydrodynamic component. Although there are no side walls to induce electrical forces in the horizontal direction, the domain width is small enough for the periodic boundary to have an effect. The ellipse interacts with itself through the periodic boundary and as the symmetry breaks a horizontal force is exerted on the ellipse. The electrical force points in the negative direction for positive angles and in positive direction for negative angels. This means that the ellipse is electrically forced to the left for positive angles and to the light for negative angles, which is also in line with hydrodynamic tendency of the ellipse. As a result, electrical and hydrodynamical forces have the same period while the electrical part slightly lags behind.

5 Conclusions

An ISPH method to simulate the sedimentation of an elliptic particle in quiescent flow under external electric field is presented here. A shifting boundary condition for long term simulation of the sedimentation is implemented and tested. It is seen that the shifting boundary condition has negligible effects in the absence of the electric field. The simulations in the presence of the electric field are carried out for two sets of electrical properties and four different boundary configurations. The results show that both electrical properties and the boundaries have significant effects on the trajectory of the sedimentation.

6 Acknowledgments

NT gratefully acknowledges financial support from Mitacs-Accelerate program grant number IT08354. MY acknowledges financial support provided by the Scientific and Technological Research Council of Turkey (TUBITAK) grant number 112M721. AS acknowledges the financial support provided by the Natural Sciences and Engineering Research Council (NSERC) for the Canada Research Chair in Computational and Experimental Mechanics.

REFERENCES

[1] Xia, Z., Connington, K.W., Rapaka, S., Yue, P., Feng, J.J. and Chen, S. Flow patterns in the sedimentation of an elliptical particle. *J. Fluid Mech.* (2009) **625**:249-272.

[2] Quincke, G. Ueber rotationen im constanten electrischen felde. *Ann. Phys.* (1896) **295**:417-486.

[3] Ai, Y., Beskok, A., Gauthier, D.T., Joo, S.W. and Qian, S. DC electrokinetic transport of cylindrical cells in straight microchannels. *Biomicrofluidics* (2009) **3**:044110.

[4] House, D.L., Luo, H. and Chang, S. Numerical study on dielectrophoretic chaining of two ellipsoidal particles. *J. Colloid Interface Sci.* (2012) **374**:141-149.

[5] Tofighi, N., Ozbulut, M., Feng, J.J. and Yildiz, M. The effect of normal electric field on the evolution of immiscible Rayleigh-Taylor instability. *Theor. Comput. Fluid Dyn.* (2016) **30**:469-483.

[6] Suzuki, K. and Inamuro, T. Effect of internal mass in the simulation of a moving body by the immersed boundary method. *Comput. Fluids* (2011) **49**:173-187.

[7] Tofighi, N., Ozbulut, M., Rahmat, A., Feng, J.J. and Yildiz, M. An incompressible smoothed particle hydrodynamics method for the motion of rigid bodies in fluids. *J. Comput. Phys.* (2015) **297**:207-220.

[8] Saville, D.A. Electrohydrodynamics: The Taylor-Melcher leaky dielectric model. *Annu. Rev. Fluid Mech.* (1997) **29**:27-64.

[9] Monaghan, J.J. Smoothed Particle Hydrodynamics and Its Diverse Applications. *Annu. Rev. Fluid Mech.* (2012) **44**:323-346.

[10] Zainali, A., Tofighi, N., Shadloo, M.S. and Yildiz, M. Numerical investigation of Newtonian and non-Newtonian multiphase flows using ISPH method. *Comput. Meth. Appl. Mech. Eng.* (2013) **254**:99-113.